High-fat diet exacerbates hepatic and adipose insulin signaling impairment and ovarian lesions in a rat model of letrozole-induced polycystic ovary syndrome

SUNJU SO, SUJIN KWON, LA YOON CHOI, DAE YONG KIM and MI HYE KIM

College of Korean Medicine, Woosuk University, Jeonju, Jeonbuk State 54986, Republic of Korea

Received June 22, 2026; Accepted August 28, 2026

DOI: 10.3892/mmr.2026.14019

Abstract. Polycystic ovary syndrome (PCOS) is a multifactorial endocrine disorder characterized by ovarian dysfunction and metabolic abnormalities, including insulin resistance. Letrozole (LET)-based animal models reproduce hyperandrogenic features but often lack the metabolic phenotype of obesity-associated PCOS. Therefore, in the present study, a high-fat diet (HFD) was combined with LET and alterations in insulin signaling in metabolic tissues were examined. Female Sprague-Dawley rats were assigned to control (CON), LET-induced PCOS (LV) and HFD plus LV (HLV) groups. Body weight, fasting glucose, serum lipids, histology of the liver, visceral adipose tissue (VAT), ovaries and uterus, pancreatic and ovarian immunofluorescence, and hepatic and VAT quantitative PCR for insulin signaling markers were evaluated. Both LV and HLV groups showed increased body weight and fasting glucose, with impaired hepatic and VAT insulin receptor (INSR)/insulin receptor substrate 1 (IRS-1)/phosphoinositide 3-kinase (PI3K)/protein kinase B (AKT) signaling relative to the CON group, with no significant differences between the LV and HLV groups for these parameters. However, HLV further increased hepatic phosphoenolpyruvate carboxykinase and glucose-6-phosphatase, and VAT sterol regulatory element-binding protein 1c and acetyl-CoA carboxylase, beyond the levels observed in the LV group, and produced more severe hepatic steatosis and adipocyte hypertrophy compared with the LV group. Ovarian cytochrome P450 family 19 subfamily A member 1 and anti-Müllerian hormone dysregulation was also more pronounced in the HLV group than in the LV group. By contrast, no significant difference was observed between the LV and HLV groups for serum lipid levels, pancreatic β-cell area or apoptosis, INSR, IRS1, IRS2, AKT, PI3K, glucose transporter 4, carnitine palmitoyltransferase 1A or acyl-CoA oxidase 1. These findings indicated that HFD selectively exacerbates specific molecular and histopathological features of PCOS beyond those induced by LET alone, partially recapitulating obesity-related PCOS and providing a practical preclinical platform for studying the metabolic-reproductive axis and evaluating interventions targeting insulin resistance.

Introduction

Polycystic ovary syndrome (PCOS) is a prevalent endocrine and metabolic disorder among women of reproductive age, with a global occurrence estimated at approximately 15-20%, contingent upon the diagnostic criteria employed (1). Clinically, PCOS is characterized by androgen excess, ovulatory dysfunction, and polycystic ovarian morphology. A significant proportion of affected individuals also display metabolic abnormalities, with roughly 70% exhibiting insulin resistance (IR), which may elevate the risk of dyslipidemia, obesity, and type 2 diabetes (2). Moreover, PCOS is associated with a range of conditions including infertility, metabolic syndrome, impaired glucose tolerance, type 2 diabetes, cardiovascular disease, depression, obstructive sleep apnea (OSA), endometrial cancer, and metabolic dysfunction-associated steatotic liver disease (MASLD) (3).

Obesity represents a significant factor that exacerbates all hormonal and metabolic characteristics of PCOS, and its prevalence is rising globally (4). Obesity-induced insulin resistance, characterized by impaired cellular response to insulin signaling, is considered a primary mechanism underpinning metabolic complications associated with PCOS (5). Hyperinsulinemia, initially arising as a compensatory response to insulin resistance, has been reported to promote hyperandrogenemia and visceral adipose tissue (VAT) dysfunction. Prolonged exposure to hyperinsulinemia contributes to β-cell stress and eventual dysfunction (6). This phenomenon is frequently accompanied by a reduction in hepatic SHBG levels in insulin-resistant PCOS (7), which is attributed to insulin directly stimulating steroidogenesis in ovarian Theca cells via PI3K-dependent activation of 17α-hydroxylase (8). Furthermore, oxidative stress and inflammation may diminish insulin signaling and augment androgen excess, thereby potentially leading to metabolic and reproductive disturbance in PCOS (9).

Correspondence to: Professor Mi Hye Kim, College of Korean Medicine, Woosuk University, 61 Seonneomeo 3-gil, Wansan, Jeonju, Jeonbuk State 54986, Republic of Korea
E-mail: kimmh526@woosuk.ac.kr

Key words: polycystic ovary syndrome, obesity, letrozole, high-fat diet

Given that the precise etiologies of PCOS remain elusive, there is a need for experimental models that replicate all reproductive and metabolic alterations associated with PCOS (10). The *in vivo* model induced by letrozole (LET) is widely used as a control for assessing relevant physiological responses. LET, an aromatase inhibitor, inhibits the conversion of androgens to estrogens, resulting in persistent hyperandrogenemia and anovulation, which mirror the primary endocrine symptoms of PCOS (11). Nevertheless, while the LET-induced PCOS model predominantly mimics reproductive disturbances, metabolic phenotypes such as insulin resistance and hepatic steatosis may be less severe than those observed with obesity-associated PCOS (12). Recent evidence indicates that the addition of a high-fat diet (HFD) to LET-induced PCOS yields an *in vivo* phenotype more akin to obesity-associated PCOS, characterized by in increased body mass, elevated testosterone levels, more profound impairment of glucose and lipid metabolism, and exacerbated insulin resistance compared to LET administration alone (13). Moreover, under these combined conditions, decreased phosphorylation of proteins involved in insulin signaling pathways, such as insulin receptor (INSR)/insulin receptor substrate (IRS)/phosphoinositide 3-kinase (PI3K)/protein kinase B (AKT) and extracellular signal-regulated kinase 1/2 (ERK1/2) was observed not only in typical insulin-sensitive tissues but also in the ovaries, suggesting a potential mechanistic link between systemic metabolic stress and ovarian dysfunction (13).

Various studies employing HFD+LET rats have demonstrated that this combined model exhibits more severe metabolic disturbances and a more detrimental inflammatory and oxidative stress environment compared with the LV group. Administration of HFD in LET-induced PCOS mice resulted in elevated fasting insulin and blood glucose levels, increased HOMA-IR and triglycerides, heightened testosterone and malondialdehyde (MDA) levels, and a reduction in high-density lipoprotein (HDL) cholesterol. These changes exacerbate insulin resistance, dyslipidemia, and oxidative stress (14). Furthermore, the combination of HFD and LET provoked significant oxidative stress and inflammatory responses, culminating in the most profound impairment in metabolic and hormonal parameters, along with heightened expression of inflammatory genes and oxidative stress markers (15). Based on prior research, the HFD+LET model more accurately stimulates obesity-related PCOS and is valuable for investigating tissue-level molecular pathways linking metabolic dysfunction to ovarian pathology. Nevertheless, despite advancements in model development, there remains a paucity of evidence concerning rat models that concurrently encompass obesity-related metabolic disturbances and ovarian pathology. Consequently, the objective of this study is to develop a rat model that more faithfully mirrors the clinical manifestation of obesity-related PCOS by incorporating metabolic stress factor such as an HFD, and to perform multi-organ assessments of the liver, VAT, pancreas, and ovaries to explore the evaluate the potential utility of targeting the metabolic-reproductive axis in preclinical PCOS research.

An unbalanced diet is a major environmental factor affecting the onset and exacerbation of PCOS. To emulate this condition in preclinical research, rodents are frequently administered a HFD to induce obesity and insulin resistance, thereby replicating associated metabolic characteristics (5). These findings suggest that the combined effect of elevated fat intake and hyperandrogenemia may compound adverse metabolic and reproductive outcomes, indicating that disruption in insulin signaling and inflammation in metabolic tissues could underpin the pathophysiology, as suggested by (16). Nevertheless, the molecular mechanism by which metabolic stress precipitates ovarian dysfunction under these combined conditions remains insufficiently understood. The liver, adipose tissue, and ovaries engage in complex interactions, with insulin signaling pathways such as IRS-1/AKT/glucose transporter 4 (GLUT4) recognized as critical components of this relationship (8). Additionally, the pancreas may serve as a pivotal nexus within this axis, since insulin secretion in response to chronic metabolic stress can result in pancreatic β-cell dysfunction, thereby intensifying systemic insulin resistance and ovarian dysfunction, as indicated by (17).

Therefore, in this study, we hypothesized that the combination of a HFD and LET administration would exacerbate impaired insulin signaling in key metabolic tissues, resulting in a concomitant aggravation of metabolic disorders and ovarian lesions. Accordingly, we seek to evaluate how HFD exacerbates metabolic dysfunction and ovarian lesions, elucidate the metabolic-reproductive axis, and confirm the role of insulin resistance in PCOS within the context of obesity. Furthermore, our objectives include not only establishing a rat model of PCOS but also to clarify how tissue-level impairment of insulin signaling is associated with reproductive abnormalities.

Materials and methods

Animal experimental design. Seven-week-old female Sprague-Dawley (SD) rats were purchased from Samtako (Osan, Korea). They were housed under conditions of 23±2˚C, 50±10% humidity, and a 12-h light and dark cycle. They had free access to food and water. After 1 week of adaptation, rats were randomly assigned to three groups (n=8): control (CON), LET-induced PCOS with normal diet (LV), and LET-induced PCOS with HFD (HLV). The CON group received oral administration of distilled water once daily for 7 weeks. The LV and HLV groups received oral administration of LET (112809-51-5, MCE, New Jersey, USA) at a concentration of 1 mg/kg, suspended in 1% carboxymethylcellulose (CMC, 9004-32-4, DuKSAN, Yongin, Korea) once daily for 7 weeks to induce PCOS. The HLV group was fed a HFD (60 kcal% fat, 20 kcal% carbohydrate, and 20 kcal% protein, total 5.24 kcal/g, D12492, Samtako, Osan, Korea) for 7 weeks, while the remaining groups were fed a normal diet. Upon completion of the experiment, the rats were placed in a clean chamber for the euthanasia procedure. The CO_2 concentration was gradually increased to 30%; once this level was reached, the rats were allowed to lose consciousness before blood was collected by cardiac puncture, followed by euthanasia via cervical dislocation. Subsequently, the ovaries, uterus, liver, pancreas, and VAT were harvested. The collected blood was centrifuged at 12,000 x g for 15 min to separate the serum, which was then stored at -80˚C. All procedures were approved by the Woosuk University Institutional Animal Care and Use Committee (approval no. WS-2024-04; Jeonju, South Korea).

Metabolic measurements. Body weight was recorded weekly during the experiment. For the oral glucose tolerance test

(OGTT), rats were fasted for 12 h before the test, and then 2 g/kg of D-glucose was orally administered. Blood glucose was measured via tail vein blood at 0, 30, 60, 90, and 120 min after the test. Furthermore, for fasting blood glucose measurement before necropsy, blood glucose was measured using a portable blood glucose meter after a 12-h fast.

Serum biochemical parameters. Serum aspartate aminotransferase (AST), alanine aminotransferase (ALT), triglycerides (TG), total cholesterol (TC), and high-density lipoprotein cholesterol (HDL-c) levels were measured using commercially available kits (Fujifilm, Tokyo, Japan) according to the manufacturer's instructions. Low-density lipoprotein cholesterol (LDL-c) levels were calculated according to the manufacturer's instructions. Absorbance was measured using a DRI-CHEM NX500 analyzer (Fujifilm, Tokyo, Japan).

Histopathological examination. Tissue samples (liver, pancreas, VAT, ovary, and uterus) were fixed in 10% neutral buffered formalin, embedded in paraffin, and then sectioned at 4 μm thickness using a Micro-Tome (HM325, Epredia, Michigan, USA). Three sections per animal were analyzed for each tissue. The sections were stained with hematoxylin and eosin (H&E) and examined under a light microscope (Eclipse Ci-L Plus, Nikon, Tokyo, Japan). For ovarian histology, H&E-stained sections were used to identify and count corpora lutea, cystic follicles, and atretic follicles was measured at x40 magnification. Morphometric parameters (corpus luteum volume, cystic follicle volume and ovarian volume) were also measured using H&E images. For VAT, adipocyte diameter was measured at x200 magnification, and hepatic steatosis and liver injury were assessed using Kleiner's non-alcoholic fatty liver disease (NAFLD; now referred to as MASLD) activity score (18) modified to include the sum of four histological components: Steatosis (0-3), lobular inflammation (0-3), hepatocyte ballooning (0-2), and fibrosis stage (0-4), yielding a total score ranging from 0 to 12 (Table I).

Table I. Histopathology score of hepatic lesions.

Histological criteria	Score
Steatosis	
<5%	0
5-33%	1
>34-66%	2
>66%	3
Inflammation	
No foci	0
<2 foci/x200	1
2-4 foci/x200	2
>4 foci/x200	3
Hepatocyte ballooning	
None	0
Few balloon cells	1
Prominent ballooning	2
Fibrosis stage	
None	0
Perisinusoidal or periportal	1
Perisinusoidal and portal/periportal	2
Bridging fibrosis	3
Cirrhosis	4

Immunofluorescence (IF) staining. Paraffin-embedded ovarian and pancreatic tissues were incubated with insulin (rabbit), anti-Müllerian hormone (AMH) (mouse), and cytochrome P450 family 19 subfamily A member 1 (CYP19A1) (rabbit) antibodies (Santa Cruz Biotechnology, Dallas, TX, USA) at a 1:500 dilution, followed by Alexa Fluor 488 and 594-conjugated rabbit and mouse IgG antibodies (Invitrogen, Thermo Fisher Scientific, Waltham, MA, USA) at a 1:1,000 dilution. Sections were then mounted using DAPI-containing mounting solution (H-1500-10, Vector Laboratories, CA, USA). Images were captured using an EVOS M5000 Imaging System (Thermo Fisher Scientific). Fluorescence intensity was quantified using ImageJ software (NIH, USA). Regions of interest (ROIs) were manually defined around pancreatic islets, and mean fluorescence intensity was measured after background subtraction. All images were captured using identical exposure settings. For each animal, non-overlapping fields were analyzed and averaged.

TUNEL assay. Apoptosis was assessed using the DeadEnd™ Fluorometric TUNEL System (G3250, Promega, WI, USA). Pancreatic sections were deparaffinized with xylene, rehydrated with ethanol, and then incubated with 20 μg/ml proteinase K at 37˚C for 20 min. The sections were then washed with PBS. A drop of detection mixture, prepared according to the manufacturer's instructions, was added and incubated at 37˚C in the dark for 60 min. After washing again with PBS, the sections were mounted using a mounting medium containing DAPI (H-1500-10, Vector Laboratories, Newark, CA, USA). TUNEL-positive nuclei were quantified using ImageJ software (NIH, Bethesda, MD, USA). Pancreatic islets were manually delineated as ROI, and DAPI-positive nuclei within each islet ROI were identified. TUNEL fluorescence intensity was measured within each nuclear ROI, and nuclei with fluorescence intensity exceeding a predefined threshold were classified as TUNEL-positive. The same threshold was applied to all images acquired under identical exposure settings.

TUNEL-positive cells (%)=number of TUNEL-positive DAPI nuclei/total number of DAPI-positive nuclei within the islet ROI x100.

Non-overlapping pancreatic islet fields per animal were analyzed, and the averaged percentage was used as the representative value for each animal.

Reverse transcription-quantitative PCR analysis of metabolic disorder-related RNA expression in liver and VAT. Total RNA was extracted from rat liver and VAT. Briefly, 50 mg of tissues were homogenized in 1 ml of Easy Blue Reagent (Intron Biotechnology, Seongnam, Korea) containing protease inhibitor cocktail using a tissue homogenizer (T 10 basic, IKA, Germany) on ice, then centrifuged at 12,000 x g for 15 min at 4˚C, and the supernatant was collected for RNA extraction

using Easy Blue Reagent (Intron Biotechnology, Seongnam, Korea) according to the manufacturer's protocol. For each sample, 5 μg of RNA was reverse transcribed into cDNA using the Prime Script RT Reagent Kit (TaKaRa Biotech, Dalian, China), and quantitative PCR was performed using TB Green PCR Master Mix (TaKaRa Biotech, Dalian, China). The target genes were IRS-1, insulin receptor substrate 2 (IRS-2), phosphoinositide 3-kinase (PI3K), carnitine palmitoyltransferase 1A (CPT1a), acyl-CoA oxidase 1 (ACOX1), AKT, GLUT4, insulin receptor (INSR), sterol regulatory element-binding protein 1c (SREBP-1c), fatty acid synthase (FAS), acetyl-CoA carboxylase (ACC), phosphoenolpyruvate carboxykinase (PEPCK), and glucose-6-phosphatase (G6Pase), with β-actin used as an internal control. Relative expression levels were calculated using the $2^{-\Delta\Delta Cq}$ method with the CON group as the calibrator (19) (Table II).

Statistical analysis. Statistical analyses were performed using GraphPad Prism 9.0 (GraphPad Software, San Diego, CA, USA). All quantitative data are presented as mean ± SD, with the exception of the NAFLD activity score, which owing to its categorical/ordinal nature, is presented as the median (interquartile range, IQR). Overall differences among three groups (CON, LV, HLV) were analyzed using one-way ANOVA, followed by Tukey's post hoc test for all pairwise comparisons, including CON vs. LV, CON vs. HLV, and LV vs. HLV, performed for every reported outcome, with the exception of the NAFLD activity score. For the NAFLD activity score, overall differences among the three groups were analyzed using the Kruskal-Wallis test, followed by Dunn's multiple comparisons test for all pairwise comparisons. For repeated-measures data (body weight and OGTT time-course curves), a two-way mixed design ANOVA (group x time) was used, with group as the between-subject factor and time as within-subject factor, followed by Tukey's multiple comparisons test performed at every time point for all three pairwise comparisons, including LV vs. HLV. P<0.05 was considered to indicate a statistically significant difference.

Results

Metabolic assessment. HFD treatment was associated with changes in body weight and serum metabolic parameters (Fig. 1). Body weight increased throughout the experimental period in both the LV and HLV groups. From week 3, both the LV and HLV groups showed significantly higher body weights compared with the CON group, with this difference becoming more pronounced from week 4 onward. By week 8, body weight was significantly higher in the LV group (330.70±24.06 g) and HLV group (346.90±40.19 g) compared to the CON group (266.20±19.81 g, P<0.0001), with no statistically significant difference between the LV and HLV groups (Fig. 1A). During the OGTT, glucose levels were elevated in both the LV and HLV groups compared with the CON group. At 0 min, both the LV and HLV groups showed significantly higher glucose levels than the CON group (P<0.05 and P<0.01, respectively). At 30 min, the HLV group had significantly higher glucose levels than the CON group (P<0.001) and the LV group (P<0.05). At 60 min, glucose levels were significantly higher in the LV group than in the CON group (P<0.05) and further elevated in the HLV group compared with both the CON (P<0.0001) and LV groups (P<0.01). At 90 and 120 min, the HLV group maintained significantly higher glucose levels than the CON group (P<0.05), whereas no significant difference between the LV and HLV groups was observed at these late time points (Fig. 1B). Fasting blood glucose levels were also significantly higher in the LV (169.40±44.77 mg/dl), and HLV (194.10±42.70 mg/dl) groups than in the CON group (110.10±11.94 mg/dl; P<0.05 and P<0.01), with no significant difference between the LV and HLV groups (Fig. 1C).

Serum TG and TC levels were higher in the LV (TG 64.71±14.96 mg/dl; TC 78.5±14.06 mg/dl) and HLV (TG 65.88±11.83 mg/dl; TC 79.38±15.8 mg/dl) groups than in CON (TG 45.8±18.67 mg/dl; TC 65.67±10.39 mg/dl; P<0.05, P<0.01, P<0.001). HDL-c levels were lower in the LV (22.00±9.25 mg/dl) and HLV (22.71±6.71 mg/dl) groups than in CON (28.57±4.11 mg/dl), whereas LDL-c levels were higher in the LV (40.17±15.73 mg/dl) and HLV (45.75±12.88 mg/dl) groups compared with CON (33.86±4.88 mg/dl; Fig. 1D). No significant difference between the LV and HLV groups was observed for any serum lipid parameter.

Furthermore, analysis of the estrous cycle via vaginal smear demonstrated regular periodicity in the CON group; the four phases of the estrous cycles were evenly distributed in contrast to the LV and HLV groups, which appeared to have ceased the estrus cycle characterized by a predominant phase at one stage and a diminished stage in the cycle. Moreover, it was confirmed that the estrous cycles of the majority of rats in the LV and HLV groups were disrupted, whereas the CON group exhibited a normal estrus cycle (Fig. 1E).

Histopathological analysis. Histopathological analysis was conducted to determine whether metabolic alterations were associated with anomalies in reproductive tissues (Fig. 2). Gross morphological evaluation revealed that both the LV and HLV groups exhibited enlarged ovaries and an increased number of blister counts compared to the CON group. This resulted in a statistically significant increase in ovarian weight in the LV group (87.23±22.6 mg) and the HLV group (89.59±14.2 mg) compared with the CON group (53.53±8.2 mg, P<0.0001). H&E staining showed normal ovarian morphology in the CON group, characterized by multiple developing follicles and multiple corpora lutea. In contrast, both the LV and HLV groups displayed hallmark features of polycystic ovaries, such as enlarged follicles and diminished numbers of corpora lutea with the LV group presenting an average of 4.87±1.2 and the HLV group (4.75±1.0, and the CON group 9.97±1.8, P<0.001). Additionally, the number of antral follicles was significantly lower in the LV group (1.25±0.5) and the HLV group (0.875±0.4) compared to the CON group (3.43±0.9, P<0.001 and P<0.0001, respectively). The prevalence of cystic follicles was elevated in the LV (5.5±1.1) and HLV groups (7.87±2.1) relative to the CON group (1.86±0.6, P<0.01 and P<0.0001). Atretic follicles were similarly increased in the LV (1.4±1.34) and HLV groups (2.5±1.22) vs. CON (0.86±0.38, P<0.01) with the HLV group showing a significant increase compared to the LV group (P<0.05). Volumetric analysis of corpora lutea and cystic follicle indicated that luteal volume in the LV group (177.34±78.42 mm^3) was reduced relative to the CON group (314.50±118.52 mm^3, P<0.05). In contrast, the

Table II. List of rat primer sequences used in quantitative PCR.

Gene	Forward primer sequence, 5'-3'	Reverse primer sequence, 5'-3'
β-actin	TCGTGCGTGACATTAAAGAG	ATTGCCGATAGTGATGACCT
IRS-1	GTGGAGTTGAGTTGGGCAGA	CCTGTCCGCATGTCAGCATA
IRS-2	TCATACCCAGCCTCATCACTCA	CTCAGGTCGGCCAACGAT
PI3K	AATACACCTGGTGCTCGACAC	CCTCTGATCTTGACCCTGAAC
INSR	CAGTGTCGTGATCGGAAGTATT	CTGAGGTACTCTGGGTTTG AAG
AKT	CAGGCACCCCTTCCTTACAG	GGTACACCACATCCCTCGAG
GLUT4	CCAGTATGTTGCGGATGCTATG	TGGTTTCAGGCACTCTTAGGA
CPT1a	TGGGGAAGAGACAGACACCA	ATCGTGGTAGAGCCAGACCT
ACOX1	GGATGGCAGTCCGGAGAATA	TGGCTTCGAGTGAGGAAGTT
SREBP-1c	GACGACGGAGCCATGGATT	GGGAAGTCACTGTCTTGGTT GTT
FAS	TCCCAGGTCTTGCCGTGC	TCGGATGCCTAGGATGTGTGC
ACC	TCCTGCTGCTATTGCTACCCCA	CAGTCCCAGCGCTCACATAA
PEPCK	GGATGTGGCCAGGATCGAAA	ATACATGGTGCGGCCTTTCA
G6Pase	TTCCGGTGCTTGAATGTCGT	GCAAGGTAGATCCGGGACAG
TNF	GTCGTAGCAAACCACCAAGC	TGTGGGTGAGGAGCACATAG
IL-1β	GGGATGATGACGACCTGCTA	TGTCGTTGCTTGTCTCTCCT
IL-18	GACAAAAGAAACCCGCCTG	ACATCCTTCCATCCTTCACAG

IRS, insulin receptor substrate; PI3K, phosphoinositide 3-kinase; INSR, insulin receptor; AKT, protein kinase B; GLUT4, glucose transporter 4; CPT1a, carnitine palmitoyltransferase 1A; ACOX1, acyl-CoA oxidase 1; SREBP-1c, sterol regulatory element-binding protein 1c; FAS, fatty acid synthase; ACC, acetyl-CoA carboxylase; PEPCK, phosphoenolpyruvate carboxykinase; G6Pase, glucose-6-phosphatase.

HLV group exhibited a partial increase (339.12±212.65 mm^3). Cystic follicle volume was significantly higher in the LV (174.73±82.47 mm^3) and HLV groups (158.51±71.36 mm^3) compared to the CON group (48.12±38.24 mm^3, P<0.05, P<0.01; respectively, Fig. 2A).

The gross morphology of the uterus indicated pronounced uterine atrophy in the LV and HLV groups. Consistently, uterine length was significantly reduced in the LV (2.10±0.8 cm) and HLV groups (2.21±0.5 cm) compared with the CON group (2.76±0.4 cm, P<0.001, P<0.0001). Histological examination further confirmed uterine atrophy. The uterine diameter was significantly decreased in the LV (249.6±52.69 μm) and HLV groups (310.88±46.56 μm) compared with the CON group (410.84±55.91 μm, P<0.0001), with the reduction being significantly less pronounced in the HLV group compared with the LV group (P<0.05; Fig. 2B).

Metabolic structural changes in the liver, pancreas, and VAT were observed sequentially (Fig. 3). The lobular architecture of the liver remained intact in the CON group, while mild hepatocyte cavitation and localized lipid droplets were observed in the LV group. The HLV group exhibited more widespread fat deposition, hepatocyte ballooning and increased inflammatory cell infiltration. MASLD activity scores exhibited a significant increase in both the LV (4.60±1.53) and HLV groups (6.67±0.52) relative to the CON group (2.60±1.58, P<0.001, P<0.0001), with the HLV group presenting a significantly higher MASLD activity score than the LV group (P<0.05). In the pancreas, the cellular density and arrangement within the islets appeared relatively uniform in the CON group. In contrast, the LV and HLV groups exhibited reduced islet size, increased intercellular spacing, and decreased cell density. In particular, the HLV group exhibited more irregular islet contours, with a tendency for the blurred boundaries between islets and acini. VAT showed clear hypertrophy, with mean adipocyte diameter increasing from 45.71±5.1 μm in the CON group to 57.38±7.5 μm in the LV group and further to 79.09±6.8 μm in the HLV group (P<0.0001), and the HLV group showing a significantly greater adipocyte diameter compared to the LV group (P<0.0001). Based on these observations, additional assessment of insulin immunofluorescence staining in pancreatic sections was conducted.

Pancreatic β-cell alteration and apoptosis. To evaluate whether metabolic disorders altered pancreatic β-cells, insulin immunofluorescence staining was conducted (Fig. 4A). In the CON group, islets showed strong, uniform insulin-positive staining with well-defined structural integrity. Conversely, insulin fluorescence intensity was markedly diminished in both the LV and HLV groups. Additionally, islets appeared smaller than those in the CON group. Quantitative analysis revealed a significant reduction in the proportion of insulin-positive areas in the LV (31.24±3.09) and HLV (30.98±6.95) groups comparison to the CON group (61.79±5.98, P<0.0001). No significant difference in insulin-positive area was observed between the LV and HLV groups.

To evaluate apoptosis within the pancreatic islets, TUNEL fluorescence staining was conducted (Fig. 4B). A minimal number of TUNEL-positive nuclei were observed within the

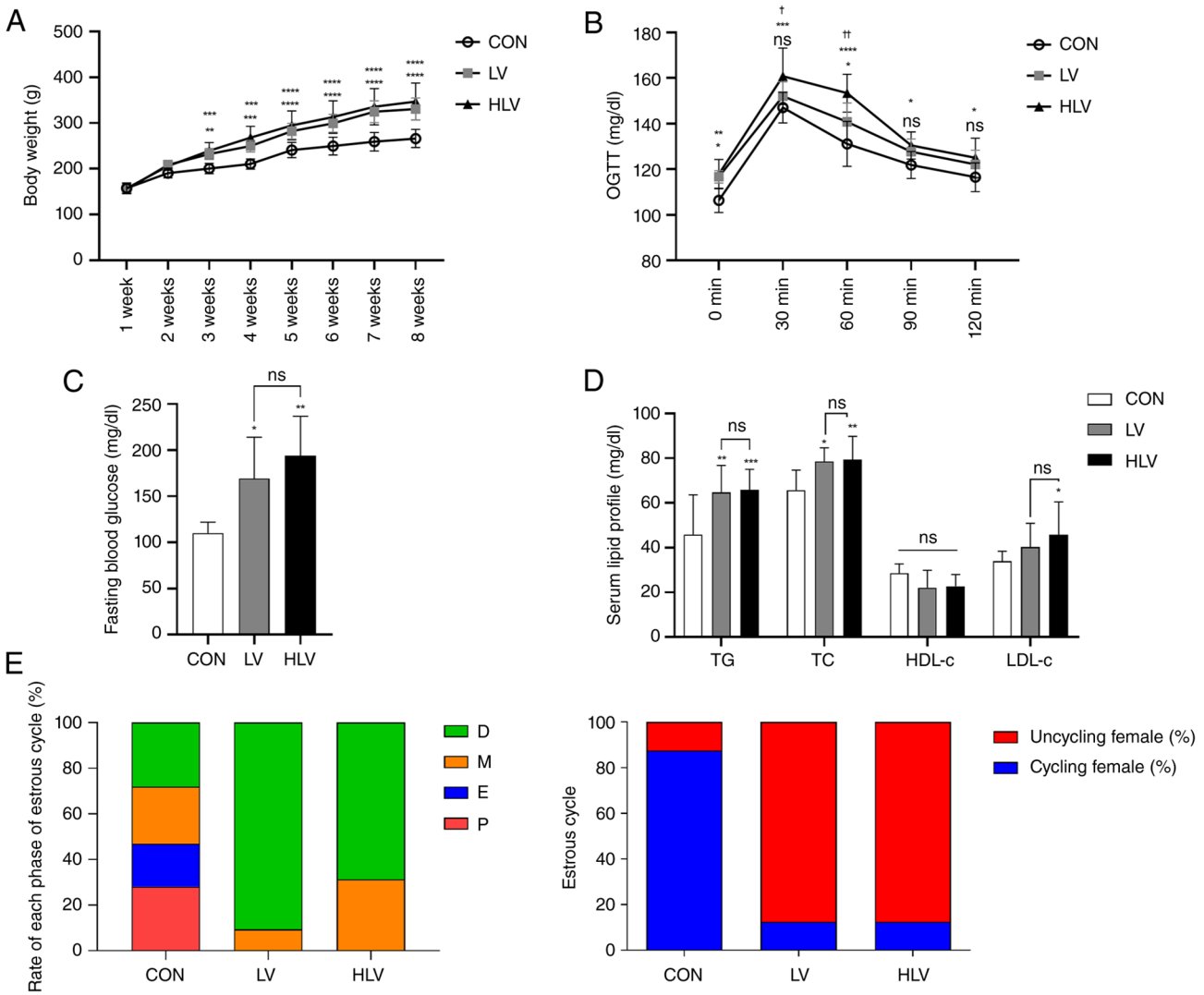

Figure 1. Metabolic and reproductive alterations in letrozole and HFD-induced PCOS rats. Rats were assigned to three groups: CON, normal diet + distilled water (p.o.); LV, LET (1 mg/kg, p.o.) with normal diet; and HLV, LET (1 mg/kg, p.o.) plus a HFD (60 kcal% fat). (A) Body weight changes during the experimental period. (B) OGTT responses. (C) Fasting blood glucose levels. (D) Serum lipid profile, including TG, TC, HDL-c and LDL-c. (E) Estrous cycle distribution presented as the ratio of time spent in each phase. Data are expressed as mean ± SD. *P<0.05, **P<0.01, ***P<0.001 and ****P<0.0001 vs. CON; †P<0.05 and ††P<0.01 LV vs. HLV; ns, non-significant pairwise comparisons. D, diestrus; E, estrus; HDL-c, high-density lipoprotein cholesterol; HFD, high-fat diet; LDL-c, low-density lipoprotein cholesterol; LET, letrozole; M, metestrus; OGTT, oral glucose tolerance test; P, proestrus; p.o., per os; TC, total cholesterol; TG, triglycerides.

pancreatic islets of the CON group, whereas a higher proportion of TUNEL-positive nuclei was detected in the LV and HLV groups. Quantitative analysis revealed that the percentage of TUNEL-positive cells was significantly increased in the LV (17.49±1.44%) and HLV (18.83±3.04%) groups compared with the CON group (8.20±3.07%, P<0.0001). With no statistically significant difference between the LV and HLV groups.

Ovarian immunofluorescence. To corroborate the alterations in steroid levels induced by LV, ovarian tissue was subjected to immunofluorescence staining for CYP19A1 and AMH (Fig. 5). In the ovaries of the CON group, CYP19A1 expression was modest and predominantly localized within the corpus luteum. However, in both the LV and HLV groups, the fluorescence intensity of CYP19A1 was significantly increased throughout the follicular region. Quantitative analysis revealed that CYP19A1 expression was significantly increased in the LV (31.46±2.22) and HLV (41.80±3.27) groups compared to the CON (18.17±0.84) group (P<0.01 and P<0.0001, respectively), with the HLV group exhibiting significantly higher CYP19A1 expression than the LV group (P<0.01). AMH expression was also elevated in the LV and HLV groups. In the ovaries of the CON group, moderate AMH staining was observed, confined to the corpus luteum, in contrast, the AMH signal was more intense and widespread in the LV (25.53±2.62) and HLV (35.82±2.94) groups. Quantitative analysis further confirmed that AMH fluorescence intensity was significantly increased in both experimental groups relative to the CON (16.69±3.60, P<0.05 and P<0.001) group, with a more pronounced elevation in the HLV group than in the LV group (P<0.05).

Gene expression analysis of insulin signaling, lipogenesis, and inflammation. Studies of hepatic insulin signaling have confirmed consistent reductions in key signaling components

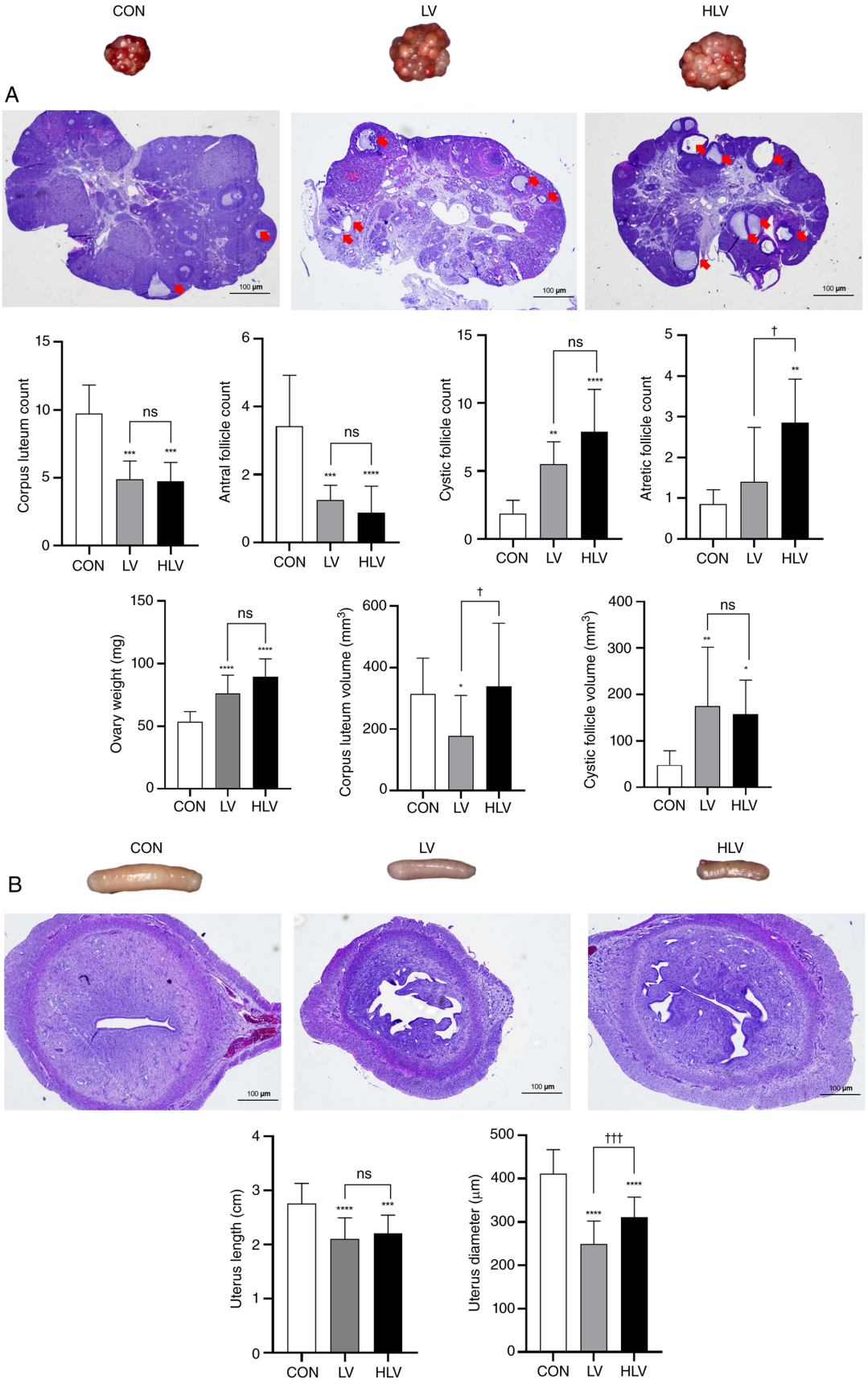

Figure 2. Ovarian polycystic morphology and uterine atrophy in letrozole and HFD-induced PCOS rats. Representative gross morphology and H&E-stained sections of reproductive tissues are shown for CON, normal diet + distilled water (p.o.); LV, LET (1 mg/kg, p.o.) with normal diet; and HLV, LET (1 mg/kg, p.o.) plus a HFD (60 kcal% fat). (A) Ovary: Gross ovarian appearance, representative H&E images (magnification, x40; scale bar=100 μm), and quantitative analysis of follicle-related parameters, including corpus luteum count, antral follicle count, cystic follicle count, and atretic follicle count, as well as ovary weight and cystic follicle volume. Red arrows indicate cystic follicles. (B) Uterus: Gross uterine appearance, representative H&E images (magnification, x20; scale bar=100 μm), and quantification of uterus length and uterus diameter. Data are expressed as mean ± SD. *P<0.05, **P<0.01, ***P<0.001 and ****P<0.0001 vs. CON; †P<0.05 and †††P<0.001 LV vs. HLV; ns, non-significant pairwise comparisons. HFD, high-fat diet; LET, letrozole; p.o., per os.

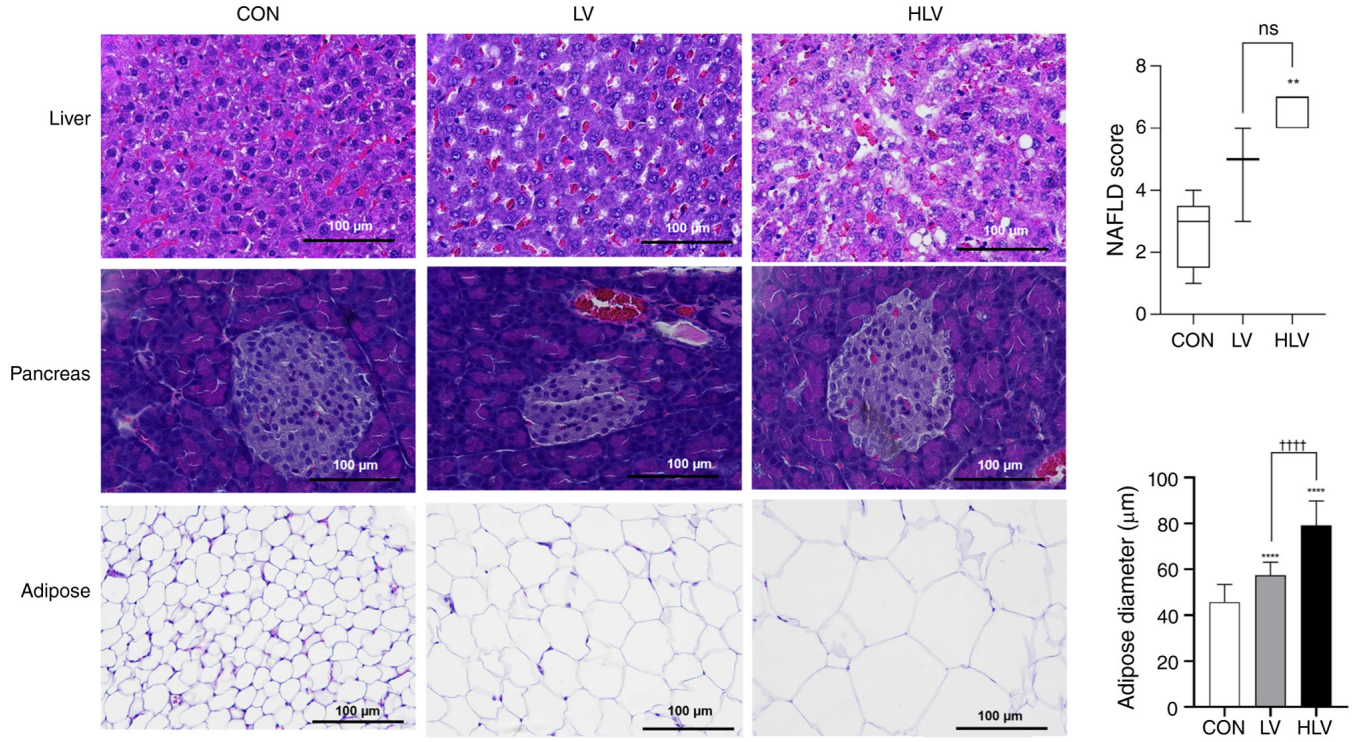

Figure 3. Effects of letrozole and HFD on histopathological changes in liver, pancreas, and adipose tissue in PCOS-induced rats. Rats were assigned to the following groups: CON, normal diet + distilled water (p.o.); LV, LET (1 mg/kg, p.o.) with normal diet; and HLV, LET (1 mg/kg, p.o.) plus a HFD (60 kcal% fat). Representative H&E-stained sections of liver, pancreas, and VAT from each group are shown (magnification, x200; scale bar=100 μm). Quantitative analyses of NAFLD (now referred to as metabolic dysfunction-associated steatotic liver disease) activity score are presented as box-and-whisker plots showing the median and interquartile range, with whiskers indicating the minimum and maximum values, and were analyzed using the Kruskal-Wallis test followed by Dunn's multiple comparisons test. VAT diameter data are expressed as mean ± SD. **P<0.01, ****P<0.0001 vs. CON; ††††P<0.0001 LV vs. HLV; ns, non-significant pairwise comparisons. HFD, high-fat diet; LET, letrozole; NAFLD, nonalcoholic fatty liver disease; p.o., per os; VAT, visceral adipose tissue.

relative to the CON group. Specifically, INSR levels decreased from 1.00±0.09 in CON to 0.57±0.21 in the LV group and further to 0.30±0.05 in the HLV group (P<0.01 for LV vs. CON; P<0.0001 for HLV vs. CON). IRS1 levels also decreased from 1.00±0.14 in CON to 0.64±0.07 in the LV and to 0.53±0.06 in HLV (all P<0.01). IRS2, another key adaptor in insulin signaling, decreased from 1.00±0.08 in the CON group to 0.74±0.09 in the LV group and 0.56±0.07 in the HLV group (P<0.05). AKT expression was also significantly decreased from 1.00±0.24 in the CON group to 0.67±0.05 in the LV group and to 0.47±0.24 in the HLV group (P<0.05). PI3K decreased from 1.00±0.18 to 0.69±0.11 in LV group and further to 0.46±0.09 in the HLV group (P<0.01 for HLV vs. CON). GLUT4 levels were significantly decreased in both LV and HLV groups (0.45±0.03 and 0.41±0.09, respectively) compared with CON group (1.00±0.12, P<0.0001; Fig. 6A). However, no significant difference between the LV and HLV groups was detected for any of these insulin signaling genes (INSR, IRS1, IRS2, AKT, PI3K, and GLUT4).

CPT1a, a gene associated with fatty acid oxidation, exhibited decreased levels, declining from 1.00±0.14 in the CON group to 0.47±0.08 in the LV group and 0.43±0.06 in the HLV group (P<0.01 for LV vs. CON; P<0.001 for HLV vs. CON). ACOX1 levels were also decreased from 1.00±0.07 to 0.47±0.04 in LV group and 0.41±0.12 in HLV group (P<0.0001; Fig. 6B). No significant difference between the LV and HLV groups was observed for CPT1a or ACOX1. Meanwhile, PEPCK levels increased from 1.00±0.03 to 1.41±0.01 in LV group and 3.29±0.02 in HLV group (all P<0.0001), with the HLV group showing a significantly greater increase than the LV group (P<0.0001). G6Pase level rose from 1.00±0.18 to 1.56±0.22 in the LV group and 2.20±0.03 in the HLV group (P<0.01 for LV vs. CON; P<0.001 for HLV vs. CON), and the HLV group also exhibited significantly higher G6Pase expression than the LV group (P<0.01; Fig. 6C). Liver inflammatory cytokines were elevated in both LV and HLV groups. TNF-α was increased from 1.00±0.04 in the CON group to 1.33±0.03 in LV and 2.05±0.44 in HLV (P<0.001), with the HLV group showing a significantly greater increase than the LV group (P<0.01). IL-1β was also significantly increased from 1.00±0.19 in CON to 2.48±0.18 in LV and 2.95±0.17 in HLV (P<0.0001), with the HLV group exhibiting a significantly higher IL-1β expression than the LV group (P<0.01). IL-18 was increased from 1.00±0.20 in CON to 2.25±0.21 in LV and 1.44±0.12 in HLV (P<0.01; P<0.0001) with the LV group exhibiting a significantly higher IL-18 expression than the HLV group (P<0.0001; Fig. 6D).

VAT showed a marked increase in lipogenic gene expression. SREBP-1c levels rose from 1.05±0.14 in CON to 2.68±0.58 in LV and 4.41±0.17 in HLV groups (P<0.001 for LV vs. CON; P<0.0001 for HLV vs. CON), with the HLV group showing a significantly greater increase compared to the LV group (P<0.001). FAS expression was also significantly increased in both LV and HLV groups (11.31±0.71 and 11.79±1.07 vs. 1.00±0.07, P<0.0001); with no significant difference between the LV and HLV groups. ACC levels increased from 1.00±0.15 in the CON group to 6.36±0.47 in LV and 12.84±2.19 in HLV groups (P<0.001 for LV vs. CON; P<0.0001 for HLV vs. CON)

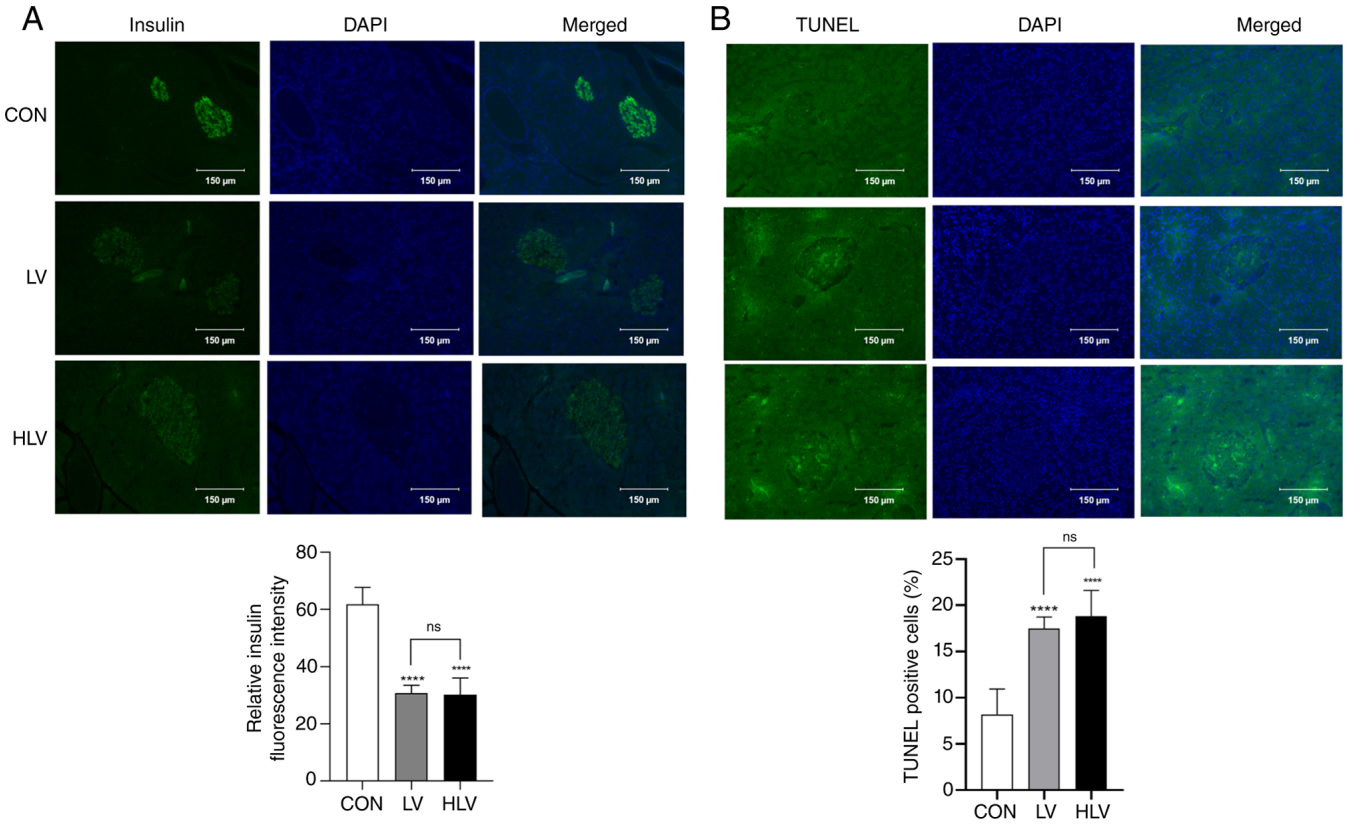

Figure 4. Effects of letrozole and HFD on pancreatic insulin expression and apoptosis in PCOS-induced rats. Rats were assigned to the following groups: CON, normal diet + distilled water (p.o.); LV, LET (1 mg/kg, p.o.) with normal diet; and HLV, LET (1 mg/kg, p.o.) plus a HFD (60 kcal% fat). (A) Representative insulin immunofluorescence images and quantitative analysis of relative insulin expression intensity are shown (magnification, x200; scale bar=150 μm). (B) Representative TUNEL staining images and quantitative analysis of the percentage of TUNEL-positive cells. Data are expressed as mean ± SD. ****P<0.0001 vs. CON; ns, non-significant pairwise comparisons. HFD, high-fat diet; LET, letrozole; p.o., per os.

and the HLV group also showed a significantly higher ACC expression to the LV group (P<0.01; Fig. 6E).

Discussion

In this study, a rat model of obese PCOS was established through the combination of LET with an HFD. This methodology is intended to better emulate the clinical spectrum of obese PCOS, characterized by mutually reinforcing metabolic and reproductive dysfunctions. While LET alone can induce hyperandrogenism and ovarian dysfunction, the inclusion of an HFD in this model resulted in more severe metabolic disturbances, such as insulin resistance, β-cell dysfunction, hepatic steatosis, and adipocyte hypertrophy (13,20). Conversely, body weight and fasting blood glucose levels did not differ significantly between the HLV and LV groups, suggesting that these systemic parameters were primarily influenced by LET-induced hyperandrogenism and were not further aggravated by HFD. Histological assessment demonstrated notable liver fat accumulation, cellular damage, and adipocyte hypertrophy. Immunostaining of pancreatic tissue confirmed a reduction in insulin-positive β-cell areas. Additionally, key components of the insulin signaling pathway, including IRS-1, AKT, and GLUT4, were showed significant reductions in liver and VAT at the molecular level relative to CON group, indicating the presence of insulin signaling disorders that were already evident in the LV group and not significantly further intensified by HFD at the transcript level, as no significant LV-HLV difference was detected for INSR, IRS-1, IRS-2, AKT, PI3K, or GLUT4.

Concomitantly, the expression of genes involved in adipogenesis SREBP-1c and ACC (significantly higher in HLV than LV) and FAS (elevated vs. CON but not significantly different between LV and HLV) and its synthesis (PEPCK, G6Pase) was increased, indicating a more extensive regulatory defect in glucose and lipid metabolism than observed in the LV group (21). In reproductive terms, this model exhibited typical ovarian features of PCOS, including decreased corpora lutea, increased follicular cysts, and abnormal ovarian morphology, suggesting follicular inactivity. These phenomena indicate an interaction between insulin resistance and ovarian dysfunction, affirming this as a phenotypic hallmark of metabolic PCOS (22). Consistent with prior studies, HFD alone causes weight gain and impaired glucose tolerance (23), while the combination of HFD with LET significantly exacerbated insulin resistance, as evidenced by elevated fasting glucose and insulin levels (23). Notably, previous research has demonstrated that the concurrent presence of HFD and hyperandrogenism leads to a more severe impairment of insulin sensitivity than either condition alone. Although earlier studies indicated LET alone typically causes only mild insulin resistance (13,24), our findings suggest that the simultaneous administration of excessive dietary fat markedly amplifies metabolic disturbances.

In the ovarian tissue of HLV rats, suppression of follicle formation, increased follicular atresia, and decreased corpora

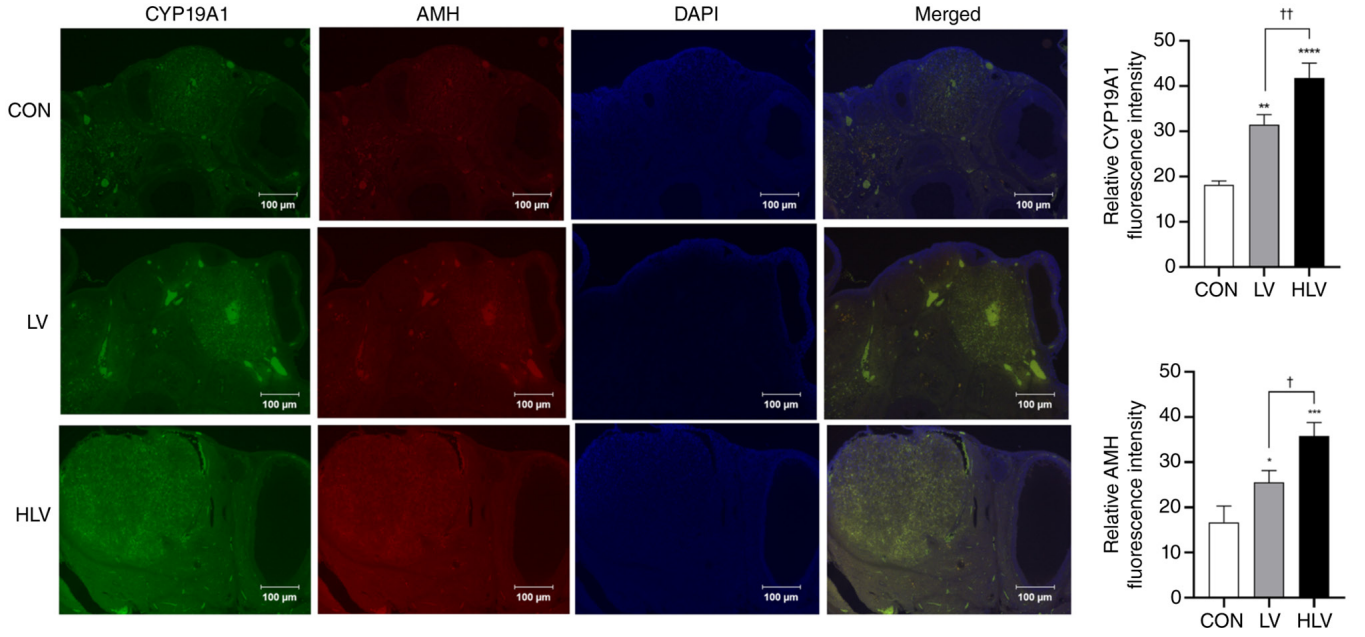

Figure 5. Effects of letrozole and HFD on ovarian CYP19A1 and AMH expression in PCOS-induced rats. Rats were assigned to the following groups: CON, normal diet + distilled water (p.o.); LV, LET (1 mg/kg, p.o.) with normal diet; and HLV, LET (1 mg/kg, p.o.) plus a HFD (60 kcal% fat). Representative immunofluorescence images of CYP19A1, AMH, DAPI, and merged ovarian sections are shown (magnification, x100; scale bar=100 μm), together with quantitative analyses of relative CYP19A1 and AMH fluorescence intensities. Data are expressed as mean ± SD. *P<0.05, **P<0.01, ***P<0.001 and ****P<0.0001 vs. CON; †P<0.05, ††P<0.01 LV vs. HLV; ns, non-significant pairwise comparisons. AMH, anti-Müllerian hormone; CYP19A1, cytochrome P450 family 19 subfamily A member 1; HFD, high-fat diet; LET, letrozole; p.o., per os.

lutea were observed, consistent with a pattern similar to that reported for LET-induced PCOS (25). Our results also confirmed the potential for an HFD to exacerbate these reproductive abnormalities, consistent with the notion that insulin resistance impairs granulosa cell function and suppresses FSH receptor signaling, thereby worsening ovarian function under metabolic stress (26). To support these results, ovarian immunofluorescence analysis revealed increased AMH and CYP19A1 signals in both the LV and HLV groups, with the strongest changes observed in the HLV group. Although these markers do not independently contribute to ovarian steroid production, the changes in their distribution and intensity suggest that the combined effects of endocrine and metabolic stress may have altered the follicular microenvironment.

The histological examination of liver tissues in the HLV group revealed both microcellular and macrocellular fat deposits that are characteristic of MASLD. This finding aligns with previous research indicating that the PCOS-HFD model exacerbates hepatic steatosis under combined metabolic and endocrine stress conditions (27,28). Molecular analysis corroborated these observations by demonstrating increased expression levels of SREBP-1c and its downstream targets, FASN and ACC (29). These molecules serve as key regulators of hepatic de novo lipogenesis and are closely linked to lipid dysregulation observed in insulin resistance (30). It is noteworthy that administration of LET alone induced only mild hepatic fat accumulation. However, when combined with an HFD, it resulted in a more pronounced fatty liver phenotype.

Pancreatic β-cell damage in HLV rats was evidenced by a significant decrease in insulin-positive areas in both the LV and HLV groups compared with CON, although neither parameter differed significantly between the LV and HLV groups. These findings indicate pancreatic islet alterations in the PCOS groups but do not establish the functional state of insulin secretion or its temporal progression. Previous studies have proposed that compensatory hyperinsulinemia associated with insulin resistance may contribute to hyperandrogenism and may eventually be followed by β-cell dysfunction (31). However, it is unclear whether this sequence occurred in this model in practice, because circulating insulin and androgen levels were not measured in the present study.

In VAT, adipocyte hypertrophy was observed in both LV and HLV groups, with a more pronounced increase in the HLV group, suggesting combined effects of excessive diet and a hyperandrogenic environment. This observation was accompanied by increased expression of adipogenic genes, including SREBP-1c, and ACC (significantly higher in HLV than LV) and FAS (elevated vs. CON but not significantly different between LV and HLV), indicating accelerated fat accumulation and a tissue state associated with local inflammation, hypoxia, and worsened systemic insulin resistance (32). It is noteworthy that our 7-week HFD protocol captures early VAT remodeling, primarily hypertrophy and lipogenic gene activation, rather than established inflammatory infiltration, which typically requires prolonged HFD feeding (16+ weeks) to become histologically evident (33). Collectively, these findings suggest that early VAT remodeling contributes to systemic insulin resistance within this model and may indirectly facilitate the progression of ovarian failure. Genetic and protein data imply that alterations in PI3K/AKT signaling in the liver and VAT of HLV rats impaired insulin signaling. In VAT, the significant reduction

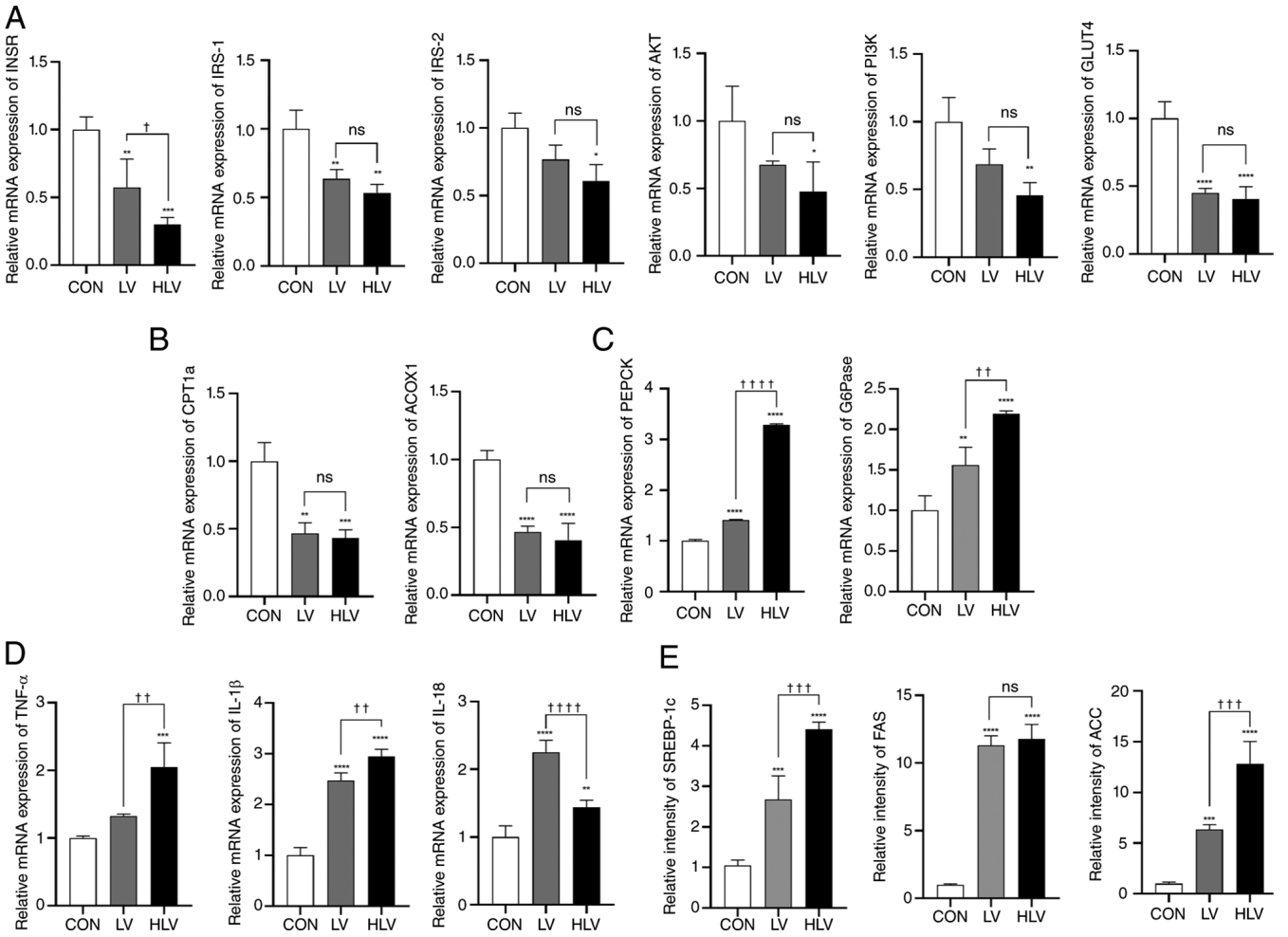

Figure 6. Quantitative PCR analysis revealed that HFD feeding profoundly altered hepatic and adipose mRNA expression profiles associated with insulin signaling, lipid metabolism, and inflammation. Rats were assigned to the following groups: CON, normal diet + distilled water (p.o.); LV, LET (1 mg/kg, p.o.) with normal diet; and HLV, LET (1 mg/kg, p.o.) plus a HFD (60 kcal% fat). (A) Relative mRNA expression levels of hepatic insulin signaling-related genes are shown. (B) Relative mRNA expression levels of hepatic fatty acid oxidation-related genes are shown. (C) Relative mRNA expression levels of hepatic gluconeogenesis-related genes are shown. (D) Relative mRNA expression levels of hepatic pro-inflammatory cytokines are shown. (E) Relative expression levels of adipose lipogenesis-related markers are shown. Data are expressed as mean ± SD. *P<0.05, **P<0.01, ***P<0.001 and ****P<0.0001 vs. CON; †P<0.05, ††P<0.01, †††P<0.001 and ††††P<0.0001 LV vs. HLV; ns, non-significant pairwise comparisons. ACC, acetyl-CoA carboxylase; ACOX1, acyl-CoA oxidase 1; AKT, protein kinase B; CPT1a, carnitine palmitoyltransferase 1A; FAS, fatty acid synthase; G6Pase, glucose-6-phosphatase; GLUT4, glucose transporter type 4; HFD, high-fat diet; INSR, insulin receptor; IRS, insulin receptor substrate; LET, letrozole; PEPCK, phosphoenolpyruvate carboxykinase; PI3K, phosphoinositide 3-kinase; p.o., per os; SREBP-1c, sterol regulatory element-binding protein 1c.

in GLUT4 expression indicates compromised insulin-stimulated glucose uptake. In the liver, hepatocytes predominantly utilize GLUT2 for bidirectional glucose transport (34). The decrease in GLUT4 mRNA may reflect low-level hepatocyte expression or contributions from hepatic non-parenchymal cell populations (35). This pattern supports broader impairment of insulin signaling across metabolic tissues rather than a specific hepatocyte glucose uptake.

This pathway is central to insulin-mediated metabolic regulation, and its downregulation may lead to decreased peripheral glucose uptake, increased hepatic glucose production, and lipotoxicity (36). Furthermore, increased expression of inflammatory cytokines, such as TNF-α, IL-1β, and IL-18, in the liver may lead to inflammation and fat accumulation in HLV rats, thereby further aggravating hepatic insulin resistance and promoting a shift toward lipogenic metabolism. Notably, TNF-α and IL-1β levels were significantly higher in the HLV group than in the LV group (P<0.01 for both; Fig. 6D), whereas IL-18 showed the opposite pattern, with significantly higher levels in the LV group (2.25±0.21) than in the HLV group (1.44±0.12; P<0.0001; Fig. 6D), although both PCOS groups remained elevated relative to CON (1.00±0.20) although this LV-HLV difference was statistically significant. Previous reports suggest that elevated hepatic G6Pase and PEPCK levels indicate increased endogenous glucose production (37). In this context, compensatory hyperinsulinemia associated with impaired glucose regulation has been proposed to promote ovarian androgen production and contribute to follicular dysfunction (38). However, as described above, whether a hyperinsulinemia-hyperandrogenism pathway occurred in the HLV group cannot be determined from the present study. Accordingly, the pancreatic β-cell alterations observed in the HLV group should be interpreted as structural evidence of islet injury rather than as evidence of a defined temporal sequence involving earlier hyperinsulinemia and subsequent

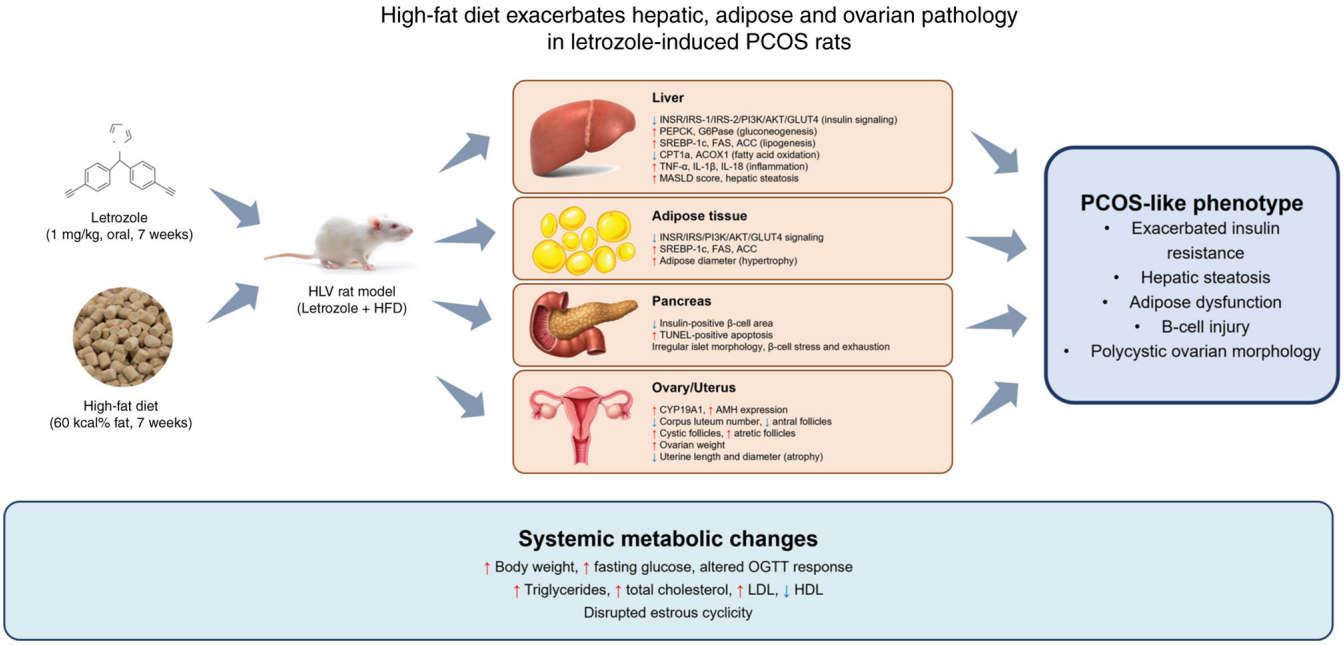

Figure 7. Schematic overview of metabolic and reproductive alterations in the HFD plus LET-induced PCOS rat model. Rats were assigned to the following groups: CON, normal diet + distilled water (p.o.); LV, LET (1 mg/kg, p.o.) with normal diet; HLV, LET (1 mg/kg, p.o.) + HFD (60 kcal% fat). Combined letrozole administration and HFD feeding were associated with impaired insulin signaling, altered glucose and lipid metabolism in the liver and visceral adipose tissue, pancreatic islet alterations, and ovarian and uterine abnormalities. Collectively, these multi-organ alterations characterize the metabolic and reproductive phenotype observed in the HLV group. HFD, high-fat diet; LET, letrozole; PCOS, polycystic ovary syndrome; p.o., per os.

β-cell decompensation. These mechanisms demonstrate how metabolic and reproductive dysfunction interlock in PCOS accompanied by obesity. Taken together, the HLV rat model is thought to more clearly reproduce the metabolic and reproductive abnormalities in obese PCOS, in contrast to the conventional model that only uses LET. Furthermore, this model can be a useful platform for preclinical evaluation of treatment strategies targeting multiple pathologies simultaneously, integrating insulin resistance, hepatic steatosis, dyslipidemia, and PCOS into a complex phenotype (39). What is remarkable about this model is that these changes are detected in multiple organs, including the liver, VAT, pancreas, and ovaries, allowing the structural and molecular aspects of the metabolism-reproduction axis to be assessed in a single experimental system. Collectively, these findings illustrate a coordinated multi-organ cascade underlying the HLV phenotype. LET-induced hyperandrogenism and HFD-induced metabolic stress jointly suppress hepatic and VAT insulin signaling, as reflected by the concurrent downregulation of INSR, IRS-1, and AKT in both tissues; this impairment is accompanied by increased hepatic gluconeogenic (PEPCK, G6Pase) and lipogenic (SREBP-1c, FASN, ACC) gene expression, promoting hepatic steatosis. In contrast, VAT GLUT4 downregulation and adipocyte hypertrophy further exacerbates peripheral insulin resistance (34-36). In parallel, pancreatic islet alterations were observed, including reduced insulin-positive area and increased apoptosis in both PCOS groups, while ovarian abnormalities were reflected by altered CYP19A1 and AMH expression, and disrupted follicular morphology. Together, these hepatic alterations with the VAT, pancreas and ovaries indicate a coordinated metabolic-reproductive phenotype in the LET and HFD model. A schematic summary of the coordinated metabolic and reproductive alterations observed in the HLV rat model is presented in Fig. 7.

Furthermore, beyond therapeutic screening, this model may also be instrumental in investigating adipokine imbalance, particularly decreased adiponectin and elevated leptin and resistin that characterize PCOS-associated VAT dysfunction. This dysfunction has been linked to endoplasmic reticulum stress and mitochondrial disturbance, which have been shown to contribute to the progression of metabolic and reproductive abnormalities in PCOS (40,41). For example, developing diverse therapeutic approaches, such as insulin-sensitizing agents like metformin, endocrine-regulating and antioxidant therapies like melatonin to alleviate oxidative stress, promoting ovarian follicle development, and modulating the gut-liver-ovarian axis through probiotics and natural product therapies-may enhance the potential to simultaneously improve metabolic balance and reproductive function (42-44). Despite these advantages, the present study has several limitations. Direct clinical application may be limited by physiological differences between rodents and humans, notably in estrous cycle dynamics, ovarian physiology, and fat distribution (45). Furthermore, although pathway-related alterations at the mRNA and protein levels have been identified, additional validation through immunohistochemistry and phosphorylation-specific markers, such as p-AKT and p-INSR, are necessary to substantiate our findings regarding impaired insulin signaling (46). Serum insulin and androgen concentrations and HOMA-IR were not directly measured in this study; therefore, the proposed pathway from compensatory hyperinsulinemia to hyperandrogenism remains hypothetical and requires future validation through

direct hormonal and metabolic assessments. Finally, future studies should focus on the temporal development and reversibility of the PCOS phenotype. Longitudinal monitoring of hormonal profiles, fertility outcomes, ovarian reserve markers such as AMH, and gut microbial communities will facilitate the elucidation of underlying mechanisms and improve cross-transferability of the findings.

In conclusion, this study effectively reproduces the key metabolic features of PCOS with LET is administered in combination with an HFD. This model provides useful experimental evidence linking insulin signaling disorders to ovarian dysfunction and may serve as a suitable preclinical platform for studying the mechanism of obesity-related PCOS evaluating treatments. However, the hypothesized pathway from compensatory hyperinsulinemia to hyperandrogenism was not directly validated by serum insulin, androgen, or HOMA-IR measurements in the present study; future studies incorporating these direct hormonal and metabolic assessments are warranted to confirm this temporal sequence.

Acknowledgements

Not applicable.

Funding

This work was supported by the National Research Foundation of Korea (NRF) grant funded by the Korea government (MSIT) (grant no. RS-2024-00338574).

Availability of data and materials

The data generated in the present study may be requested from the corresponding author.

Authors' contributions

MHK contributed to conception and design of the study. SS, SK and LYC analyzed and investigated the data. LYC, DYK and MHK contributed to the histopathological evaluation and interpretation of the experimental data. LYC, DYK and MHK confirm the authenticity of all the raw data. SS drafted the manuscript. MHK and DYK contributed to revising the manuscript and provided supervision throughout the project. All authors read and approved the final manuscript.

Ethics approval and consent to participate

The animal study was reviewed and approved by the Institutional Animal Care and Use Committee of Woosuk University (approval no. WS-2024-04).

Patient consent for publication

Not applicable.

Competing interests

The authors declare that they have no competing interests.

References

1. Daniele S, Chelucci E, Scarfò G and Artini PG: Molecular research on polycystic ovary syndrome (PCOS). Biomedicines 11: 1358, 2023.
2. Sir-Petermann T, Echiburú B, Crisosto N, Maliqueo M and Bravo FP: Metabolic features across the female life span in women with PCOS. Curr Pharm Des 22: 5515-5525, 2016.
3. Kempegowda P, Melson E, Manolopoulos KN, Arlt W and O'Reilly MW: Implicating androgen excess in propagating metabolic disease in polycystic ovary syndrome. Ther Adv Endocrinol Metab 11: 2042018820934319, 2020.
4. O'Connor A, Gibney J and Roche HM: Metabolic and hormonal aspects of polycystic ovary syndrome: The impact of diet. Proc Nutr Soc 69: 628-635, 2010.
5. Diamanti-Kandarakis E and Dunaif A: Insulin resistance and the polycystic ovary syndrome revisited: An update on mechanisms and implications. Endocr Rev 33: 981-1030, 2012.
6. Dunaif A: Insulin action in the polycystic ovary syndrome. Endocrinol Metab Clin North Am 28: 341-359, 1999.
7. Qu X and Donnelly R: Sex hormone-binding globulin (SHBG) as an early biomarker and therapeutic target in polycystic ovary syndrome. Int J Mol Sci 21: 8191, 2020.
8. Dupont J and Scaramuzzi RJ: Insulin signalling and glucose transport in the ovary and ovarian function during the ovarian cycle. Biochem J 473: 1483-1501, 2016.
9. Zeber-Lubecka N, Ciebiera M and Hennig EE: Polycystic ovary syndrome and oxidative stress-from bench to bedside. Int J Mol Sci 24: 14126, 2023.
10. Walters KA, Allan CM and Handelsman DJ: Rodent models for human polycystic ovary syndrome. Biol Reprod 86: 149, 1-12, 2012.
11. Maliqueo M, Sun M, Johansson J, Benrick A, Labrie F, Svensson H, Lönn M, Duleba AJ and Stener-Victorin E: Continuous administration of a P450 aromatase inhibitor induces polycystic ovary syndrome with a metabolic and endocrine phenotype in female rats at adult age. Endocrinology 154: 434-445, 2013.
12. Woods SC, Seeley RJ, Rushing PA, D'Alessio D and Tso P: A controlled high-fat diet induces an obese syndrome in rats. J Nutr 133: 1081-1087, 2003.
13. Xu J, Dun J, Yang J, Zhang J, Lin Q, Huang M, Ji F, Huang L, You X and Lin Y: Letrozole rat model mimics human polycystic ovarian syndrome and changes in insulin signal pathways. Med Sci Monit 26: e923073, 2020.
14. Zheng YH, Xu Y, Ma HX, Liang CJ and Yang T: Effect of high-fat diet on the intestinal flora in letrozole-induced polycystic ovary syndrome rats. Evid Based Complement Alternat Med 2021: 6674965, 2021.
15. Mirseyyed SF, Zavareh S, Nasiri M and Hashemi-Moghaddam H: An experimental study on the oxidative status and inflammatory levels of a rat model of polycystic ovary syndrome induced by letrozole and a new high-fat diet. Int J Fertil Steril 18: 45-53, 2023.
16. Zhang H, Yi M, Zhang Y, Jin H, Zhang W, Yang J, Yan L, Li R, Zhao Y and Qiao J: High-fat diets exaggerate endocrine and metabolic phenotypes in a rat model of DHEA-induced PCOS. Reproduction 151: 431-441, 2016.
17. Hasnain SZ, Prins JB and McGuckin MA: Oxidative and endoplasmic reticulum stress in β-cell dysfunction in diabetes. J Mol Endocrinol 56: R33-R54, 2016.
18. Kleiner DE, Brunt EM, Van Natta M, Behling C, Contos MJ, Cummings OW, Ferrell LD, Liu YC, Torbenson MS, Unalp-Arida A, *et al*: Design and validation of a histological scoring system for nonalcoholic fatty liver disease. Hepatology 41: 1313-1321, 2005.
19. Livak KJ and Schmittgen TD: Analysis of relative gene expression data using real-time quantitative PCR and the 2(-Delta Delta C(T)) method. Methods 25: 402-408, 2001.
20. Decourt C, Watanabe Y, Evans MC, Inglis MA, Fisher LC, Jasoni CL, Campbell RE and Anderson GM: Deletion of androgen receptors from kisspeptin neurons prevents PCOS features in a letrozole mouse model. Endocrinology 164: bqad077, 2023.
21. Knebel B, Haas J, Hartwig S, Jacob S, Köllmer C, Nitzgen U, Muller-Wieland D and Kotzka J: Liver-specific expression of transcriptionally active SREBP-1c is associated with fatty liver and increased visceral fat mass. PLoS One 7: e31812, 2012.
22. Diamanti-Kandarakis E: Polycystic ovarian syndrome: Pathophysiology, molecular aspects and clinical implications. Expert Rev Mol Med 10: e3, 2008.

23. Liu Z, Patil IY, Jiang T, Sancheti H, Walsh JP, Stiles BL, Yin F and Cadenas E: High-fat diet induces hepatic insulin resistance and impairment of synaptic plasticity. PLoS One 10: e0128274, 2015.
24. Skarra DV, Hernández-Carretero A, Rivera AJ, Anvar AR and Thackray VG: Hyperandrogenemia induced by letrozole treatment of pubertal female mice results in hyperinsulinemia prior to weight gain and insulin resistance. Endocrinology 158: 2988-3003, 2017.
25. Noorafshan A, Ahmadi M, Mesbah SF and Karbalay-Doust S: Stereological study of the effects of letrozole and estradiol valerate treatment on the ovary of rats. Clin Exp Reprod Med 40: 115-121, 2013.
26. Robker RL, Akison LK, Bennett BD, Thrupp PN, Chura LR, Russell DL, Lane M and Norman RJ: Obese women exhibit differences in ovarian metabolites, hormones, and gene expression compared with moderate-weight women. J Clin Endocrinol Metab 94: 1533-1540, 2009.
27. Lai H, Jia X, Yu Q, Zhang C, Qiao J, Guan Y and Kang J: High-fat diet induces significant metabolic disorders in a mouse model of polycystic ovary syndrome. Biol Reprod 91: 127, 2014.
28. Kanuri G and Bergheim I: In vitro and in vivo models of non-alcoholic fatty liver disease (NAFLD). Int J Mol Sci 14: 11963-11980, 2013.
29. Ferré P and Foufelle F: Hepatic steatosis: A role for de novo lipogenesis and the transcription factor SREBP-1c. Diabetes Obes Metab 12 (Suppl 2): S83-S92, 2010.
30. Dongiovanni P, Stender S, Pietrelli A, Mancina RM, Cespiati A, Petta S, Pelusi S, Pingitore P, Badiali S, Maggioni M, *et al*: Causal relationship of hepatic fat with liver damage and insulin resistance in nonalcoholic fatty liver. J Intern Med 283: 356-370, 2018.
31. De Leo V, Musacchio MC, Cappelli V, Massaro MG, Morgante G and Petraglia F: Genetic, hormonal and metabolic aspects of PCOS: An update. Reprod Biol Endocrinol 14: 38, 2016.
32. Trayhurn P: Hypoxia and adipose tissue function and dysfunction in obesity. Physiol Rev 93: 1-21, 2013.
33. Turner N, Kowalski GM, Leslie SJ, Risis S, Yang C, Lee-Young RS, Babb JR, Meikle PJ, Lancaster GI, Henstridge DC, *et al*: Distinct patterns of tissue-specific lipid accumulation during the induction of insulin resistance in mice by high-fat feeding. Diabetologia 56: 1638-1648, 2013.
34. Chadt A and Al-Hasani H: Glucose transporters in adipose tissue, liver, and skeletal muscle in metabolic health and disease. Pflugers Arch 472: 1273-1298, 2020.
35. Kurabayashi A, Furihata K, Iwashita W, Tanaka C, Fukuhara H, Inoue K, Furihata M and Kakinuma Y: Murine remote ischemic preconditioning upregulates preferentially hepatic glucose transporter-4 via its plasma membrane translocation, leading to accumulating glycogen in the liver. Life Sci 290: 120261, 2022.
36. Ramachandran V and Saravanan R: Glucose uptake through translocation and activation of GLUT4 in PI3K/Akt signaling pathway by asiatic acid in diabetic rats. Hum Exp Toxicol 34: 884-893, 2015.
37. Sun Y, Liu S, Ferguson S, Wang L, Klepcyk P, Yun JS and Friedman JE: Phosphoenolpyruvate carboxykinase overexpression selectively attenuates insulin signaling and hepatic insulin sensitivity in transgenic mice. J Biol Chem 277: 23301-23307, 2002.
38. Wu S, Divall S, Nwaopara A, Radovick S, Wondisford F, Ko C and Wolfe A: Obesity-induced infertility and hyperandrogenism are corrected by deletion of the insulin receptor in the ovarian theca cell. Diabetes 63: 1270-1282, 2014.
39. Patel R and Shah G: High-fat diet exposure from pre-pubertal age induces polycystic ovary syndrome (PCOS) in rats. Reproduction 155: 141-151, 2018.
40. Zeng X, Huang Q, Long SL, Zhong Q and Mo Z: Mitochondrial dysfunction in polycystic ovary syndrome. DNA Cell Biol 39: 1401-1409, 2020.
41. Siemers KM, Klein AK and Baack ML: Mitochondrial dysfunction in PCOS: Insights into reproductive organ pathophysiology. Int J Mol Sci 24: 13123, 2023.
42. Shpakov AO: Improvement effect of metformin on female and male reproduction in endocrine pathologies and its mechanisms. Pharmaceuticals (Basel) 14: 42, 2021.
43. Tamura H, Takasaki A, Taketani T, Tanabe M, Kizuka F, Lee L, Tamura I, Maekawa R, Asada H, Yamagata Y and Sugino N: Melatonin as a free radical scavenger in the ovarian follicle. Endocr J 60: 1-13, 2013.
44. Basnet J, Eissa MA, Cardozo LLY, Romero DG and Rezq S: Impact of probiotics and prebiotics on gut microbiome and hormonal regulation. Gastrointest Disord (Basel) 6: 801-815, 2024.
45. Chusyd DE, Wang D, Huffman DM and Nagy TR: Relationships between rodent white adipose fat pads and human white adipose fat depots. Front Nutr 3: 10, 2016.
46. Thomas GV, Horvath S, Smith BL, Crosby K, Lebel LA, Schrage M, Said J, De Kernion J, Reiter RE and Sawyers CL: Antibody-based profiling of the phosphoinositide 3-kinase pathway in clinical prostate cancer. Clin Cancer Res 10: 8351-8356, 2004.